Hindawi
Advances in Civil Engineering
Volume 2022, Article ID 1811795, 16 pages
https://doi.org/10.1155/2022/1811795

Research Article

Investigation of *p-y* Behaviors of a Cyclic Laterally Loaded Pile in Saturated Silty Sand

Sung-Ha Baek[1] **and Joonyoung Kim**[2]

[1]*School of Civil and Environmental Engineering & Construction Engineering Research Institute, Hankyong National University, Anseong, Republic of Korea*
[2]*Department of Artificial Intelligence, Hannam University, Daejeon, Republic of Korea*

Correspondence should be addressed to Joonyoung Kim; jykim91@hnu.kr

Received 8 March 2022; Accepted 25 July 2022; Published 5 December 2022

Academic Editor: Tzu-Kang Lin

This study aimed to evaluate the *p-y* behavior of pile foundations installed in saturated silty sand subject to cyclic lateral loading. Model piles were installed in saturated silty sand with three relative densities (40%, 70%, 90%), and lateral loads of three magnitudes were repeatedly applied. The model test results revealed that as the cyclic lateral loading was applied to the piles, the soil around the piles became densified in the loose soil (relative density of 40%), and the stiffness of the *p-y* curve increased. In contrast, in dense soil (relative density of 70% and 90%), the stiffness of the *p-y* curve decreased as the soil around the piles was disturbed. Special attention was devoted to the development of static and cyclic *p-y* curves for assessing the lateral behavior of offshore pile foundations installed in saturated silty sand. A comparison between the *p-y* curves derived in this study and the existing *p-y* curves for silica sand revealed that the existing *p-y* curves were more likely to overestimate the lateral load capacity of a pile installed in silty sand.

1. Introduction

In keeping pace with the global expansion of environmentally friendly green energy development, the South Korean government is promoting the "Southwest Jeollabuk-do Offshore Wind Power Project" to develop an offshore wind farm with a capacity of 2.46 GW (able to supply electricity to 2.24 million households) until 2028 by investing a total of USD 11 billion. Consequently, the construction of a 400 MW offshore wind farm is scheduled to begin in December of 2022 in an area near Wi Island in the Southwest Sea of Korea (in Jeollabuk-do), and research is underway for the safe design and construction of offshore wind turbines.

Pile foundations are widely applied to support offshore wind turbines. Compared to onshore structures, offshore wind turbines experience relatively small vertical loads but receive dominant cyclic lateral loads induced by wind, waves, and tides. Therefore, to achieve the stable performance of offshore wind structures, it is necessary to evaluate the lateral behavior of pile foundations and use these behaviors as a dominant design factor.

Among various methods for evaluating the lateral behavior of piles, the *p-y* curve method, which defines the relationship between the soil reaction (p) and displacement (y) of the soil-pile interface according to depth, is widely adopted. The *p-y* curve method models a soil-pile system with the pile and soil acting as an elastic beam and nonlinear spring, respectively, and the nonlinear spring is defined by the initial stiffness (k_{ini}) and ultimate soil reaction (p_u) of the *p-y* curve. To date, the *p-y* curve presented by O'Neill and Murchinson [1] and recommended in the API [2] (hereafter referred to as the "API *p-y* curve") has been most widely adopted in granular soils.

However, the API *p-y* curve was derived based on field tests conducted under limited conditions and has a limitation in that it cannot accurately predict the lateral behavior of a pile under arbitrary conditions (e.g., soil, pile, and load

conditions). To overcome this limitation, many researchers have evaluated the *p-y* behavior of piles installed in granular soil by conducting model pile tests under various conditions [3–6]. Kim et al. [3] applied lateral static load to model piles and evaluated the effects of the pile installation method and diameter on the *p-y* behavior of the piles. Furthermore, Choo and Kim [4] and Lee et al. [6] analyzed the *p-y* behavior of large-diameter piles through centrifugal model tests and found that the results considerably differed from the API *p-y* curve.

Overall, many researchers [3–7] have evaluated the pile behaviors installed in granular soil, but the results were derived based on model tests conducted on soils classified as sand (SP) according to the Unified Soil Classification System (USCS). There are few studies evaluating the *p-y* behavior of piles in sandy soils containing fine particles such as silty sand (SM), which are widely distributed on the seabed. Even when evaluating the lateral behavior of piles installed in silty sand, the *p-y* curve proposed for granular soil classified as SP has been applied. However, as the particle size of granular soil has a significant effect on the resistance behavior of the soil [8], soil-pile interaction behaviors also appear differently. Han et al. [9] pointed out that the current design method uses the representative *p-y* curve regardless of the type of sandy soil, but the different particle sizes of granular soil result in differences in stiffness within the elastic region. Furthermore, the initial stiffness of the *p-y* curves derived from two soils with similar relative densities (Jumunjin standard sand and Australian silty sand) differed significantly. In other words, to evaluate the behavior of a pile installed in silty sand appropriately, it is necessary to apply *p-y* curves for piles installed in silty sand during the design phase.

To consider the cyclic loading effect on laterally loaded piles, API *p-y* curve applies a reduction factor to degrade the soil resistance in static *p-y* curves. LeBlanc et al. [10] and Nicolai and Ibsen [11] performed long-term cyclic lateral load tests on a rigid model pile in the sand and found that the cyclic lateral loads always increased the soil stiffness around the pile head. On the other hand, in the model test by Zhu et al. [12], the moment unloading stiffness of a suction caisson installed in fine silty sand did not appear to be affected by the number of cyclic loads. Long and Vanneste [13] reported that cyclic lateral loads may actually increase the soil resistance due to soil densification based on full-scale cyclic lateral load tests in various types of sandy soil. Baek et al. [5] show that the stiffness of a rock-socketed pile with sand deposits increases or decreases due to the cyclic lateral loads according to the relative density of the model ground. As such, the effects of cyclic loading on pile behavior have not yet been fully understood, showing diverse trends with pile diameter, installation methods, and the type of soil.

The lateral behaviors of a pile analyzed based on *p-y* method are very sensitive to the *p-y* curves used in its design. The selection of adequate *p-y* curves is one of the most crucial factors when using this methodology to analyze laterally loaded piles [14]. Thus, it is necessary to analyze the effects of lateral behavior and cyclic loading on the silty sand that is widely distributed in the soil of the target area with a particular focus on changes in soil stiffness. In this study, we performed 1g model pile tests which applied lateral loads repeatedly on model piles. Model piles were preinstalled in saturated silty sand which has rarely been covered in previous relevant studies. Based on the model test results, we analyzed the *p-y* behavior of piles, deriving the static and cyclic *p-y* curves for silty sand. A comparison was then made between the results of this study and those of previous studies performed on SP soils. The remainder of this paper is organized as follows. Sections 2 and 3 describe our experimental method and the conditions of the model pile tests. Section 4 analyzes the model test results. Section 5 proposes a *p-y* curve based on the test results. Section 6 compares the test results with existing *p-y* curves. Finally, Section 7 summarizes this study and presents our conclusions.

2. Test Setup

2.1. Test Equipment. The model pile tests conducted in this study were performed in a cuboid model soil box with a width of 600 mm, length of 1800 mm, and height of 1200 mm (Figure 1). The four sides of the soil box were fabricated from transparent reinforced acrylic with a 20 mm thickness so that the height of the soil layer could be visually observed when the model soil was deposited layer by layer.

Table 1 lists the dimensions of the prototype and model piles used in this study. Steel pipe pile used for a foundation structure in offshore wind farm projects (e.g., Beatrice Offshore Wind Farm in Scotland) was selected as the prototype. To consider the size effects of the model tests, downscale simulations were performed by applying the 1g similitude law proposed by Iai [15]. The model piles were fabricated from aluminum pipes with an outer diameter of 30 mm, thickness of 2 mm, and length of 1,400 mm. It is a common practice to socket a pile into the bedrock to ensure end bearing capacity in areas with insufficient skin friction in granular soil, so that rock-socketed pile was simulated by fixing the bottom (tip) of the pipe to the soil box. Based on the limitation of applicable model pile materials, it was impossible to satisfy the similitude relationships of the elastic modulus, thickness, and flexural rigidity of the prototype and model simultaneously. In this study, the flexural rigidity similitude relationship of the prototype and model was satisfied by adjusting the thickness of the aluminum pipe with an elastic modulus of 70 GPa to 2 mm because the flexural rigidity has a dominant impact on the lateral behavior. This relationship was satisfied at the expense of the relationships for the elastic modulus and thickness of the pile.

Rao et al. [16] reported that a lateral load subjected to a pile influences the surrounding ground up to a radius of 10 times the pile diameter from the pile center. Therefore, this study adopted a center spacing of adjacent piles and distance from the pile centers to the wall of the soil box of 300 mm (10 times the applied outer diameter of the model pile of 30 mm). In other words, four piles with the same dimensions were installed simultaneously and model pile tests were performed, as illustrated in Figure 1.

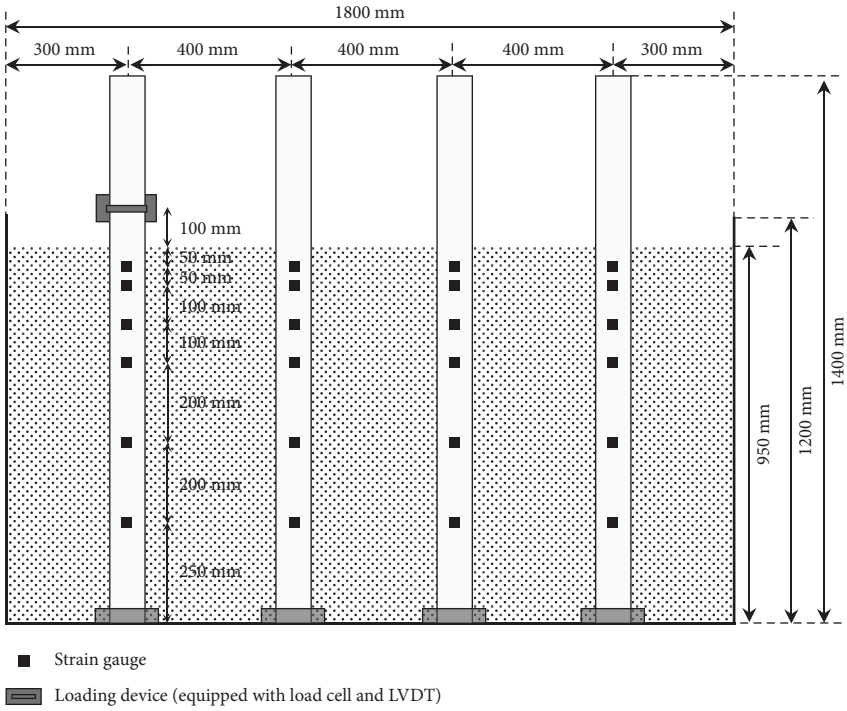

Figure 1: Schematic drawing of the model pile test setup.

Table 1: Material properties of the prototype pile and model pile used in this study.

	Scale factor	Prototype	Model ($\lambda = 15$)
Outside diameter (mm)	λ	450	30
Length (mm)	λ	21,000	1,400
Embedded depth (mm)	λ	14,250	950
Thickness (mm)	λ	40	2
Elastic modulus (GPa)	λ	210	70
Flexural rigidity (Nm^2)	$\lambda^{4.5}$	$2.29E+4$	$1.19E-1$

A lateral static load and cyclic lateral load were applied from a height of 100 mm from the ground surface through a displacement-controlled lateral loading device. A free-head condition that did not restrain the rotation of the pile head was applied. The lateral load and displacement were measured by the load cell, and a linear variable differential transformer (LVDT) was attached to the loading device when applying the lateral loads to the model piles. Additionally, the strain was measured through the attached strain gauges to the surface of the model piles at depths of 50, 100, 200, 300, 500, and 700 mm from the surface, and the results were used to evaluate the lateral behavior (p-y behavior) at different depths. The load, displacement, and strain were measured every two seconds using a static data logger at a static condition.

2.2. Model Ground. In this study, the properties of the model soil were determined by referring to ground investigation results from an area near Wi Island in the southwest Sea of Korea (hereafter referred to as the "target area") for the Southwest Jeollabuk-do Offshore Wind Power Project [17]. The results of a borehole field test conducted in sandy layers at the six locations are shown in Table 2 and the particle size distribution analysis results of the samples taken from the surface soil (0 to 15 m from the surface) are presented in Figure 2. The target area consists of loose to very dense sand layers at depths of 13.0 to 34.0 m from the ground surface, and the sand layers are classified as silty sand (SM) according to the USCS. In other words, one can see that when prototype steel pipe piles are installed in the target area, they will penetrate into both loose and very dense silty sands.

Because it is difficult to obtain large quantities of soil samples from the target area, which is under the sea, similar samples that can simulate the target soil were collected from the Saemangeum landfill site (located in Buan-gun, Jeollabuk-do, Korea). The Saemangeum landfill site is approximately 40 km from the target area in the same sea area (southwest sea), and the landfill was formed using marine dredged soil. The particle size distribution curve and index properties of the soil sample collected from the Saemangeum landfill site (hereafter referred to as "Saemangeum silty sand") are summarized in Figure 2 and Table 3, respectively. The Saemangeum silty sand is classified as SM, whose particle size distribution curve lies in the middle of the particle size distribution curves of samples from the target area. As shown in Figure 2, the Saemangeum silty sand consists of 62.7% of sand and 37.2% of silty (less than 0.1% of clay), and its mean effective particle size (D_{50}) is 0.08 mm. Furthermore, the proportion of materials that passed No. 200 sieve was 37.3%, which is much higher than the proportion of materials that passed No. 200 sieve of 0% to 5% for sandy soil classified as SP.

Target soils with loose, medium density, and very dense conditions were simulated by constructing Saemangeum soil

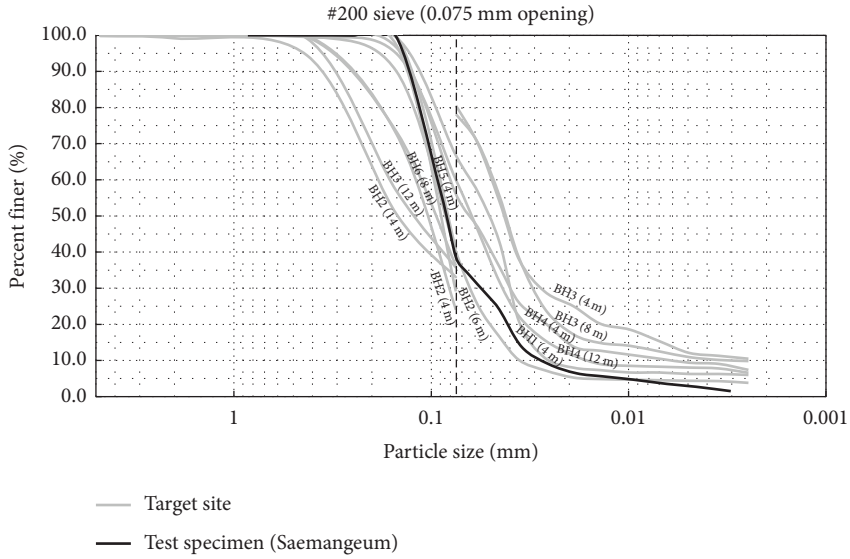

Figure 2: Particle size distribution of samples collected from the target area and Saemangeum landfill site.

Table 2: Borehole test results for the target area.

Borehole no.	Depth (m)	SPT N values (blow/cm)	Soil packing [18]
BH1	0.0~32.0	28/30–50/24	Compact to very dense
BH2	0.0~34.0	14/30–50/18	Compact to very dense
BH3	0.0~15.7	38/30–50/14	Dense to very dense
BH4	0.0~13.0	15/30–50/14	Compact to very dense
BH5	0.0~13.5	4/30–50/26	Loose to very dense
BH6	0.0~27.0	26/30–50/13	Compact to very dense

Table 3: Index properties of Saemangeum silty sand.

USCS	SM
Specific gravity, G_s	2.67
Maximum dry density, $\gamma_{d(\max)}$ (t/m^3)	1.61
Minimum dry density, $\gamma_{d(\min)}$ (t/m^3)	1.19
Effective particle size, D_{10} (mm)	0.03
Mean effective particle size, D_{50} (mm)	0.08
Coefficient of uniformity, C_u	3.42
Percent finer than #200 sieve (%)	37.3%

samples with relative densities of 40%, 70%, and 90%. The triaxial compression test revealed friction angles of 33.9°, 37.5°, and 40.2°, respectively (assuming zero cohesion). The model soils were formed in seven layers (five layers of 150 mm thickness and two layers of 100 mm thickness) for a total depth of 950 mm. First, the amount of dry sample required to form each layer of the model soil was prepared with consideration of the volume and relative density of each layer. Similar to a previous study conducted by Yang [19], the sample was then soaked in water for 10 days to fully saturate the sample. Then, wet sand was poured into a soil box filled with water and compacted using a rammer layer by layer. The measured relative densities of the preinstalled aluminum cans at various positions during soil deposition verified the homogeneity of the model soil.

3. Test Procedure and Conditions

Table 4 lists the conditions for the 12 model pile tests conducted in this study. As mentioned previously, up to four piles could be installed simultaneously, considering the dimensions of the soil box and model piles and the influential radius of the pile's lateral behavior. Therefore, model pile tests were conducted by repeating the setup processes three times.

After forming the model soil, a lateral static load was applied to one of the piles first to evaluate the static lateral load capacity (H_{us}) and p-y curve at each relative density of the model ground (T1, T5, and T9). Many researchers [20–22] have proposed criteria to determine the static lateral load capacity from a lateral load-displacement curve. This study applied the failure criteria proposed by Fleming et al. [22], which considers the occurrence of displacement by 10% of the pile diameter as the ultimate state, assuming that the pile cross-section is circular. The lateral load-displacement curve for determining the static lateral load capacity was obtained using the load cell and a linear variable differential transformer (LVDT) attached to the loading device (see Figure 1).

Thereafter, loads ($0.3H_{us}$, $0.6H_{us}$, $0.9H_{us}$) corresponding to 30%, 60%, and 90% of the static lateral load capacity (H_{us}) were applied in a two-way to the remaining three piles (Figure 3) to

Table 4: Model pile testing conditions.

Test no.	Soil conditions	Lateral loading conditions (magnitude of cyclic load)
T1	Loose state ($D_r = 40\%$)	Static loading
T2 to T4		Cyclic loading ($0.3H_{us}$, $0.6H_{us}$, $0.9H_{us}$)
T5	Medium-dense state ($D_r = 70\%$)	Static loading
T6 to T8		Cyclic loading ($0.3H_{us}$, $0.6H_{us}$, $0.9H_{us}$)
T9	Very dense state ($D_r = 90\%$)	Static loading
T10 to T12		Cyclic loading ($0.3H_{us}$, $0.6H_{us}$, $0.9H_{us}$)

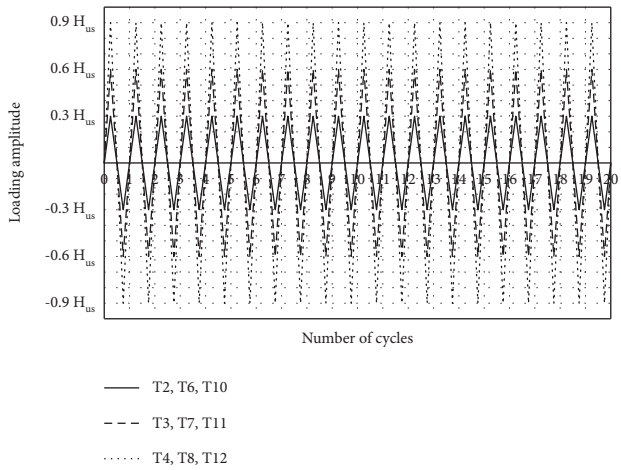

Figure 3: Sequence of cyclic lateral loads.

evaluate the cyclic *p-y* curve for each condition (T2 to T4, T6 to T8, and T10 to T12). According to Barton [23], the influence of cyclic lateral loading on the laterally loaded piles mostly appears during early cyclic loading, and its effect is less pronounced after 10 repetitions. Therefore, the number of cyclic lateral loading applications was set to 20 in this study, and the loads were slowly applied at a rate of 0.03 mm/s to prevent excess pore water pressure in the model soil.

4. Test Results and Discussion

4.1. Static p-y Behavior. The strain was measured by the strain gauges attached to the surface of the model piles at depths of 50, 100, 200, 300, 500, and 700 mm from the surface. Using the measured strain, *p-y* curves were derived at each depth using the simple beam theory [24] (equations (1)–(3)). First, the measured strain was converted into a moment using the following equation:

$$M = \frac{EI\varepsilon}{x}, \tag{1}$$

where E, I, and x denote the elastic modulus of the pile, the moment of inertia, and distance to the neutral axis, respectively, and M and ε denote the moment and strain, respectively.

Interpolation methods for obtaining a continuous moment function ($M(z)$) for the pile penetration depth (z) based on the moment obtained from a discrete location at which a strain gauge is attached include the polynomial method, cubic spline method, and weighted residual method. In this study, the continuous moment function was obtained by applying the cubic spline interpolation method, which has been applied in many studies to evaluate the lateral behavior of piles [5, 19, 25, 26]. The soil reaction (p) was calculated by differentiating the obtained moment function twice, as shown in equation (2). Then, as shown in equation (3), the moment divided by the flexural rigidity (EI) of the pile was integrated twice to calculate the displacement (y), finally resulting in the *p-y* curve.

$$p = \frac{d^2M(z)}{dz^2}, \tag{2}$$

$$y = \iint \frac{M(z)}{EI} dz, \tag{3}$$

Figure 4 presents the *p-y* curves obtained through the above process when the static lateral load is applied. The *p-y* curve shows a nonlinear hyperbolic shape. As the relative density and depth of the soil increase, the confining pressure of the soil also increases, thereby increasing the initial stiffness (slope) and maximum soil reaction (asymptotic value) of the *p-y* curve.

Figures 5–7 present the *p-y* curves from the model test results together with the *p-y* curves obtained using the API [2] method, which is most widely applied to granular soil. The API [2] method provides a very stiff elastic response and the maximum soil reaction is mobilized at a low displacement level. The high initial stiffness values and subsequent

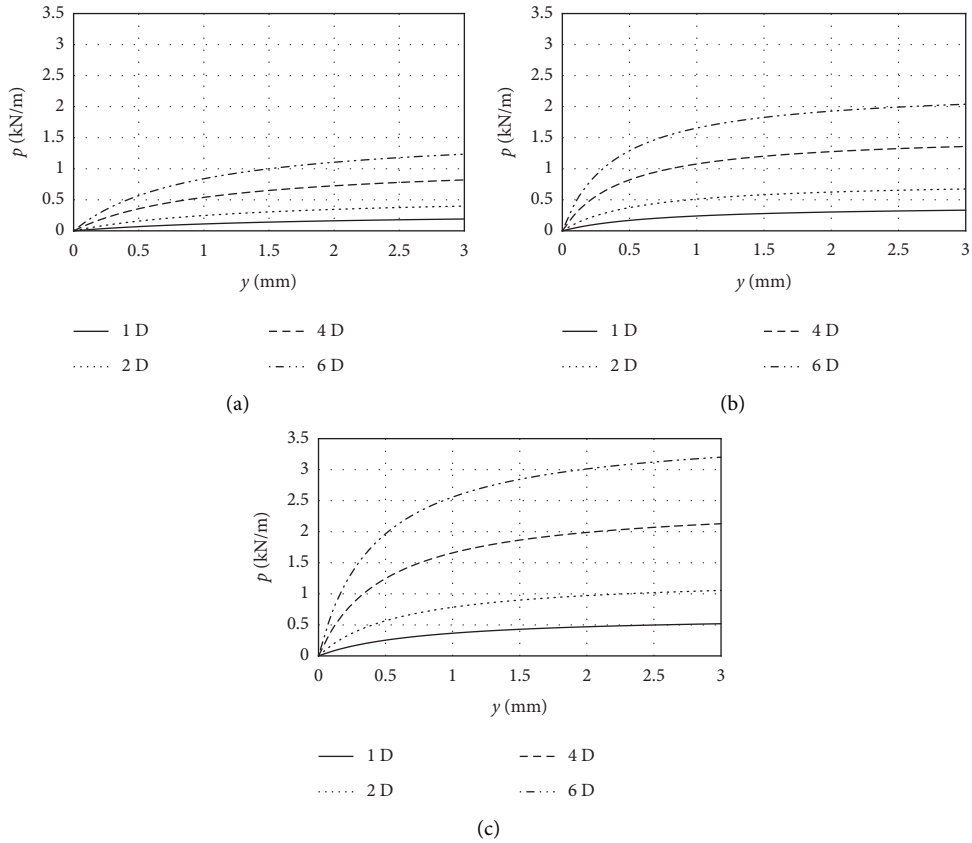

Figure 4: Experimental static p-y curves at depths of 1D, 2D, 4D, and 6D. (a) 40%. (b) 70%. (c) 90%.

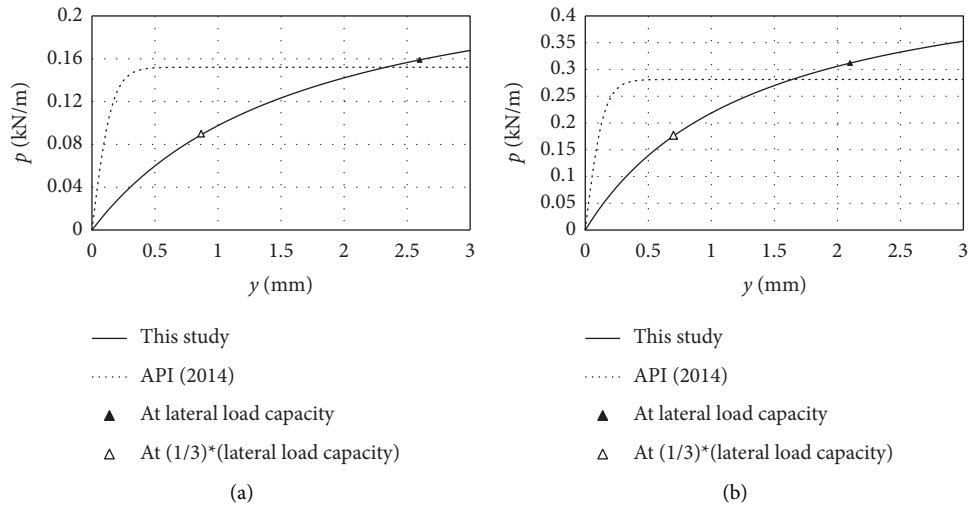

Figure 5: Continued.

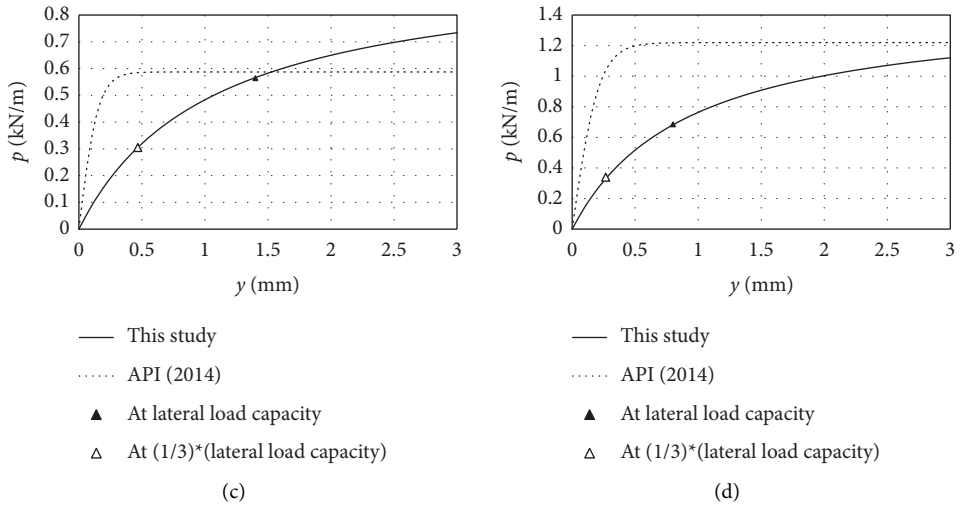

Figure 5: Comparison between experimental static p-y curves and API p-y curves (relative density of 40%): (a) 1D, (b) 2D, (c) 4D, and (d) 6D.

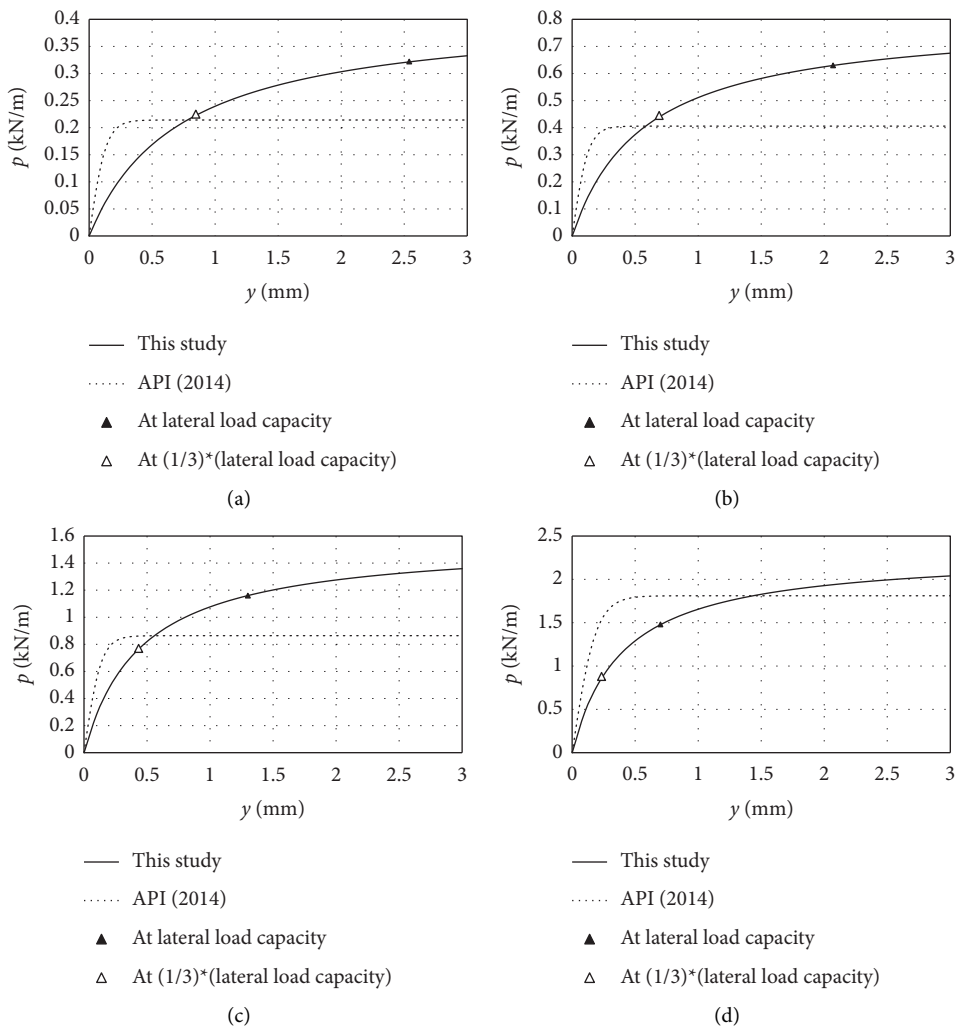

Figure 6: Comparison between experimental static p-y curves and API p-y curves (relative density of 70%): (a) 1D, (b) 2D, (c) 4D, and (d) 6D.

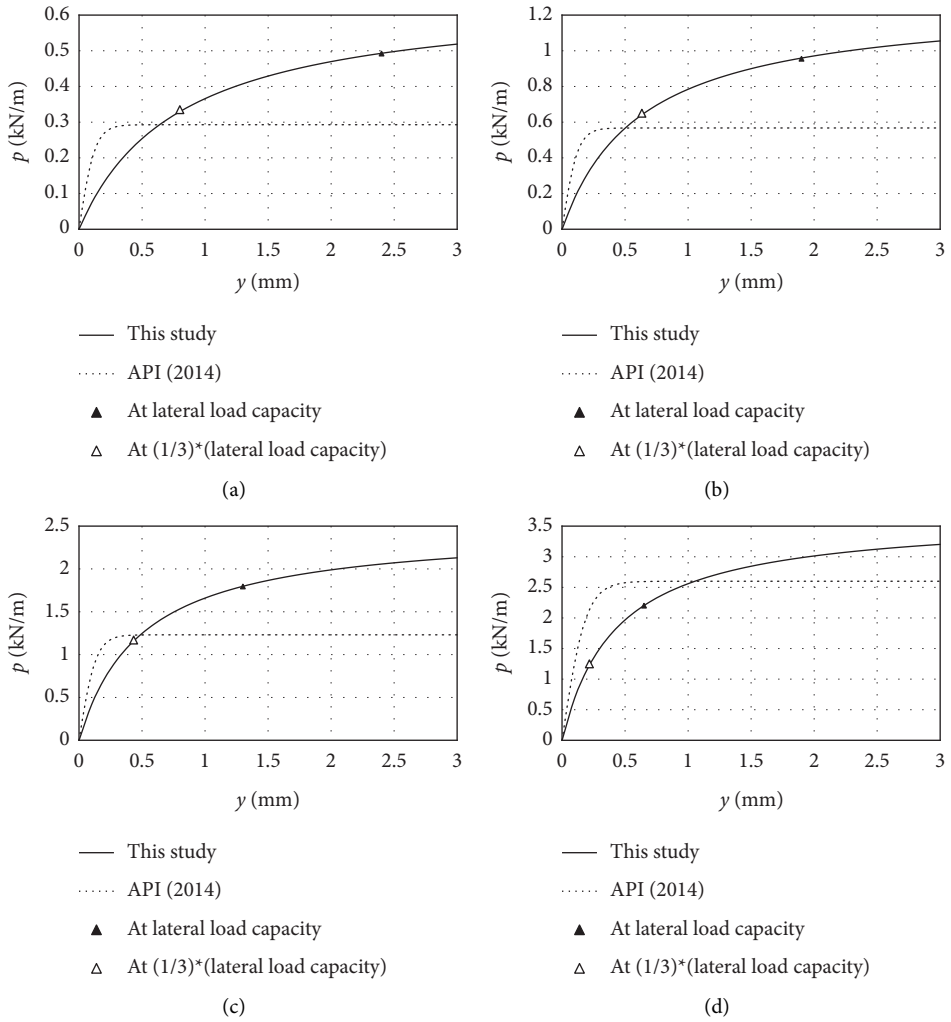

Figure 7: Comparison between experimental static p-y curves and API p-y curves (relative density of 90%): (a) 1D, (b) 2D, (c) 4D, and (d) 6D.

perfectly plastic behavior are attributed to the shear behavior of the silica sand used in API [2]; this finding is consistent with previous studies [5, 6, 27, 28]. Consequently, when the displacement of the pile was relatively small (i.e., the load applied to the pile was relatively small), the API p-y curve overestimated the soil reaction, and when the displacement was large, it underestimated the soil reaction. The closed and open symbols in the graphs in Figures 5–7 indicate the displacement and soil reaction that occurs at a load level of the static lateral load capacity and at a load level of a third of that, respectively, for the different soil density levels. According to Yoon et al. [29], the equivalent safety factors (i.e., average load factor/resistance factor) of the foundation structure suggested in offshore wind turbine design standards based on the limit state design method [30–32] are 1.50 to 2.06. The standard design for the foundation structure of South Korea [33] applies a safety factor of 3.0 to the ultimate loads based on the allowable stress design method. In other words, a load that is much lower than the ultimate bearing capacity (e.g., one-third of the static lateral capacity at a safety factor of 3.0) is considered in offshore wind power foundation design, and it can be expected that a smaller load will be experienced in actual service load conditions. Therefore, the API [2] method is likely to overestimate the soil reaction under service load conditions.

4.2. Cyclic p-y Behavior. The p-y curve during cyclic loading was derived through the same process as that for calculating the p-y curve under lateral static loading (equations (1)–(3)). Figure 8 presents the p-y curve derived from a depth of twice the pile diameter (2D) when a load with a magnitude corresponding to 60% of the static lateral capacity is repeatedly applied to the pile, as well as the p-y curve during static loading.

It was observed that the stiffness of the p-y curve increases as a cyclic lateral load is applied to the pile in the soil with a relative density of 40%, whereas the opposite phenomenon was observed in the soils with relative densities of 70% and 90%. In every test condition, the cyclic lateral load effect was the largest during early cyclic loading. However, it was insignificant after 7 to 10 cycles (changes in secant

stiffness caused by cyclic loading were within 0.5%), which was consistent with the finding presented by Barton [23].

This phenomenon appears to be a result of the soil around the piles becoming densified during cyclic lateral loading, leading to an improvement in bearing capacity in loose soil (relative density 40%), whereas the soil around the piles is disturbed (a phenomenon in which the soil in the loading direction is bulged and the soil in the opposite direction to the loading is placed in an active state is repeated) in dense soil (relative density of 70% and 90%), resulting in a reduced bearing capacity. This trend is the same as a result of a pile model test conducted in granular soil classified as SP by Baek et al. [34]. This result contradicts that of the API [2] method, which considers cyclic loading effects by applying a reduction factor to the ultimate soil reaction evaluated during static tests, regardless of the ground conditions. This demonstrates that the API *p-y* curve does not accurately consider the cyclic lateral loading effect.

Figure 9 presents the 20th cycle of *p-y* curves derived at depths of twice and six times the pile diameter translated in the *x*-axis as much as the permanent displacement due to the previous cyclic loads, as well as the static *p-y* curves at the same depth. The changing trends of the initial stiffness of the *p-y* curves caused by the cyclic loading effect can be confirmed. This effect appeared more clearly when the cyclic load was larger and closer to the surface. This is because a large lateral displacement of the soil around the piles occurs in the conditions described above, which changes the soil bearing capacity to a significant degree. Quantitative analysis of the cyclic loading effect is presented in greater detail in the next chapter.

5. Development of *p-y* Curves for Saturated Silty Sand

5.1. Static p-y Curves. This study quantitatively derived the initial stiffness (k_{ini}) and ultimate soil reaction (p_u) of the experimentally obtained *p-y* curves using the hyperbolic (equation (4)) presented by Kondner [35], which is widely applied to represent the nonlinear stress-strain relationship of soil [3, 5, 6, 19]. The k_{ini} and p_u values by depth were derived through a process of finding the best-fit curve with the experimentally obtained *p-y* curve by depth using the following equation:

$$p = \frac{y}{(1/k_{ini}) + (y/p_u)}. \quad (4)$$

As indicated by the increasing stiffness trend with a depth of the *p-y* curve in Figure 4, k_{ini} and p_u increase with the distance from the ground surface. In this study, the k_{ini} and p_u values derived by depth were curve-fitted using equation (5), which was proposed by Palmer and Thompson [36], and equation (6), which was proposed by Kim et al. [3].

$$k_{ini} = k_h (z/D)^n, \quad (5)$$

$$(p_u/D) = AK_p \gamma' z^m, \quad (6)$$

where z denotes the depth from the ground surface (m), D denotes the pile diameter (m), K_p and γ' denote the passive Earth pressure coefficient and effective unit weight (kN/m^3) of soil, respectively, k_h denotes the horizontal soil reaction constant (kN/m^2), and A, n, and m denote the dimensionless curve-fitting parameters. Additionally, D, K_p, and γ' in equations (5) and (6) are the values obtained from the test conditions, and k_{ini} and p_u are the values obtained by depth from the model test results, from which the optimal k_h, A, n, and m values are derived.

The k_{ini} and p_u values obtained by depth (z) under the test conditions (D, K_p, γ') were substituted in equations (5) and (6), and linear regression analysis was performed in the logarithm plane (Figure 10). The optimal values of k_h, A, n, and m derived as a result of our analysis are listed in Table 5. The initial stiffness and ultimate soil reaction of the *p-y* curve can be determined by substituting the optimal values of k_h, A, n, and m into equations (5) and (6). Based on these values, the lateral behavior of a pile installed in the saturated silty sand and subjected to lateral static loading can be evaluated.

5.2. Cyclic p-y Curves. This study derived a cyclic *p-y* backbone curve that can be used in the pseudostatic analysis of a pile that is subjected to cyclic loading based on the *p-y* backbone curve method proposed by Ting et al. [37]. The process of the *p-y* backbone curve method is illustrated in Figure 11.

As shown in Figure 11, the peak values of the *p-y* curves during the 20th cyclic loading were derived from each magnitude of the cyclic load. The vertices of the *p-y* loops in Figure 9 become the peak soil reaction points in Figure 11. The peak soil reaction points are then extrapolated using the same hyperbolic equation (equation (4)) used for static *p-y* fitting to derive the cyclic *p-y* backbone curve. The derived cyclic *p-y* backbone curves include the cyclic loading effect and can be defined by the initial stiffness and ultimate soil reaction, similar to the static *p-y* curves that were proposed previously.

To consider how the cyclic loading effect appears to vary with depth, the initial stiffness ($k_{ini(c)}$) and ultimate soil reaction ($p_{u(c)}$) of the cyclic *p-y* backbone curve was normalized by the k_{ini} and p_u values of the static *p-y* curve. Figure 12 presents the normalized initial stiffness ($k_{ini(c)}/k_{ini}$) and ultimate soil reaction ($p_{u(c)}/p_u$) versus the normalized depth (z/D). As mentioned previously, the change in the stiffness of the *p-y* curve under the cyclic lateral load is the greatest near the surface and gradually decreases as the depth increases. In the soil with 40% relative density, the initial stiffness and ultimate soil reaction of the *p-y* curve increase by 15.2% and 17.1%, respectively, near the surface. In contrast, in the soil with 70% relative density, the initial stiffness and ultimate soil reaction decrease to 80.8% and 74.4%, respectively. In the soil with 90% relative density, the initial stiffness and ultimate soil reaction decrease to 74.0% and 70.1%, respectively. In other words, the greater the relative density, the more clearly the stiffness reduction in the *p-y* curve caused by ground disturbance. Furthermore, the ultimate soil reaction changes more than the initial

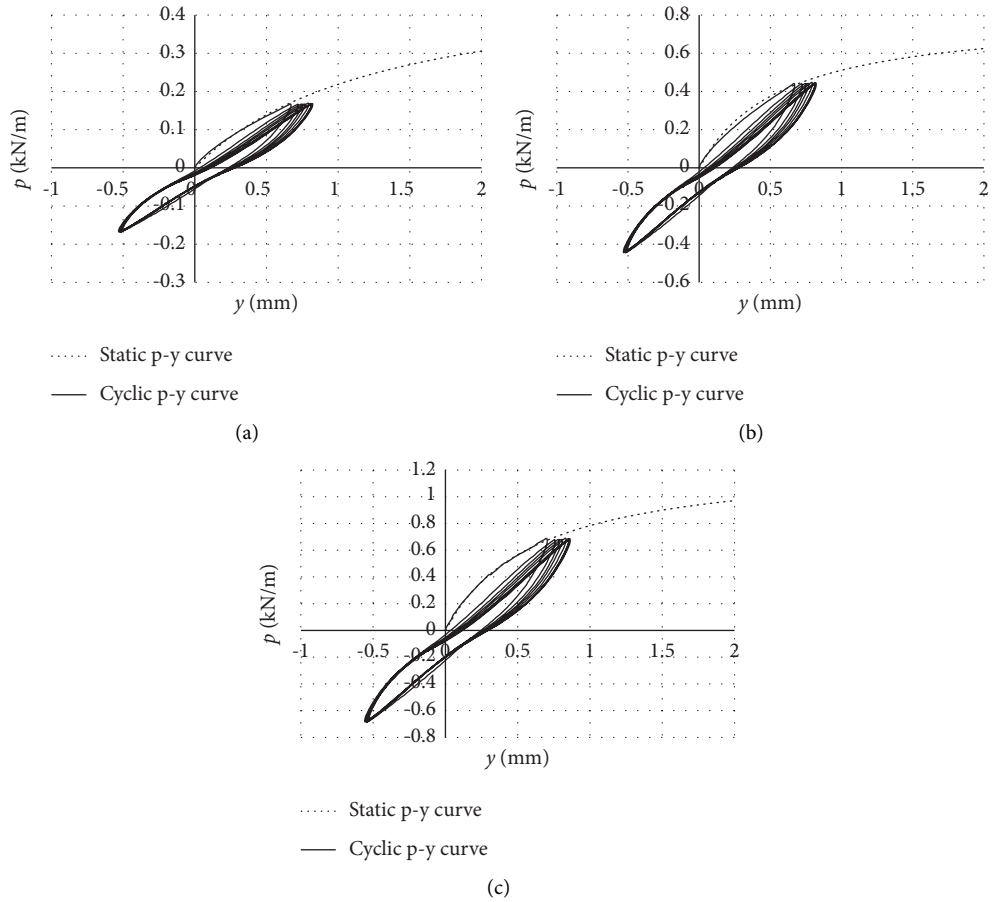

Figure 8: Experimental cyclic p-y curves at a depth of $2D$ (loading amplitude of $0.6H_{us}$). (a) 40%. (b) 70%. (c) 90%.

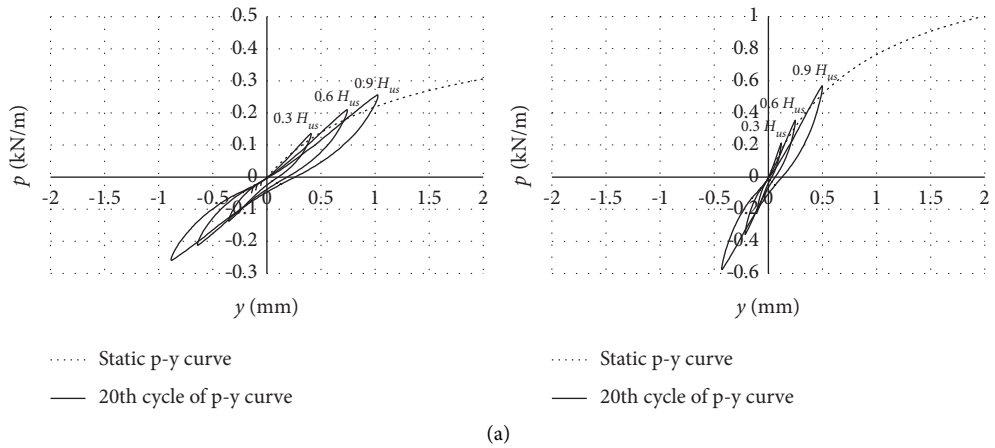

Figure 9: Continued.

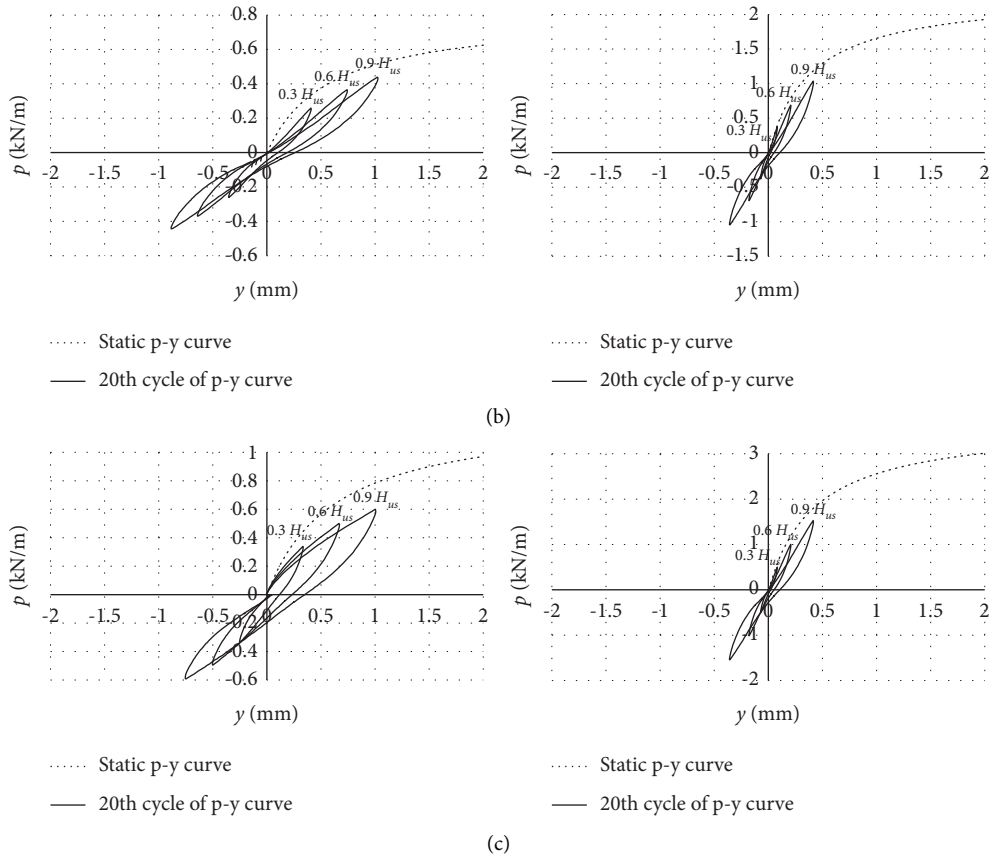

Figure 9: Comparison between 20th cycle of p-y curves and experimental static p-y curves at depths of 2D (left) and 6D (right). (a) 40%. (b) 70%. (c) 90%.

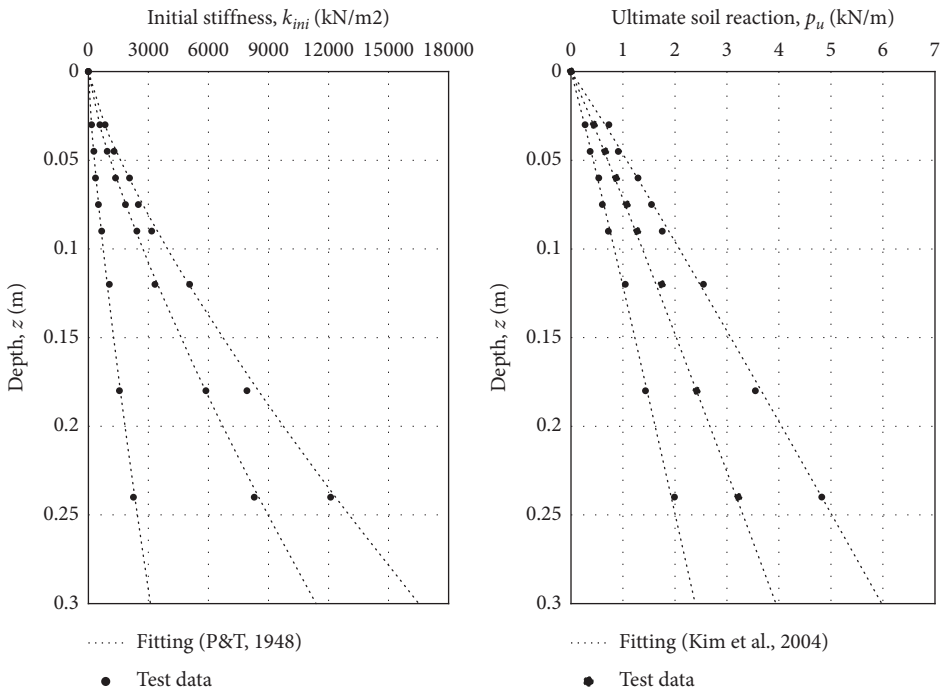

Figure 10: Initial stiffness (k_{ini}) and ultimate soil reaction (p_u) with depth.

Table 5: Backcalculated subgrade modulus and curve-fitting parameters for static p-y curves.

Soil conditions	k_h (kN/m^2)	n	A	m
Loose state ($D_r = 40\%$)	155.49		8.82	
Medium-dense ($D_r = 70\%$)	570.22	1.30	10.87	0.96
Dense state ($D_r = 90\%$)	827.51		14.33	

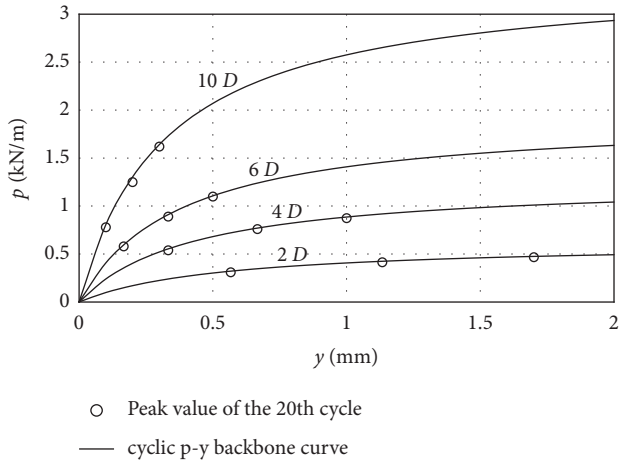

Figure 11: Peak values of the 20th cycle of p-y loops and their backbone curves at depths of 2D, 4D, 6D, and 10D ($D_r = 70\%$).

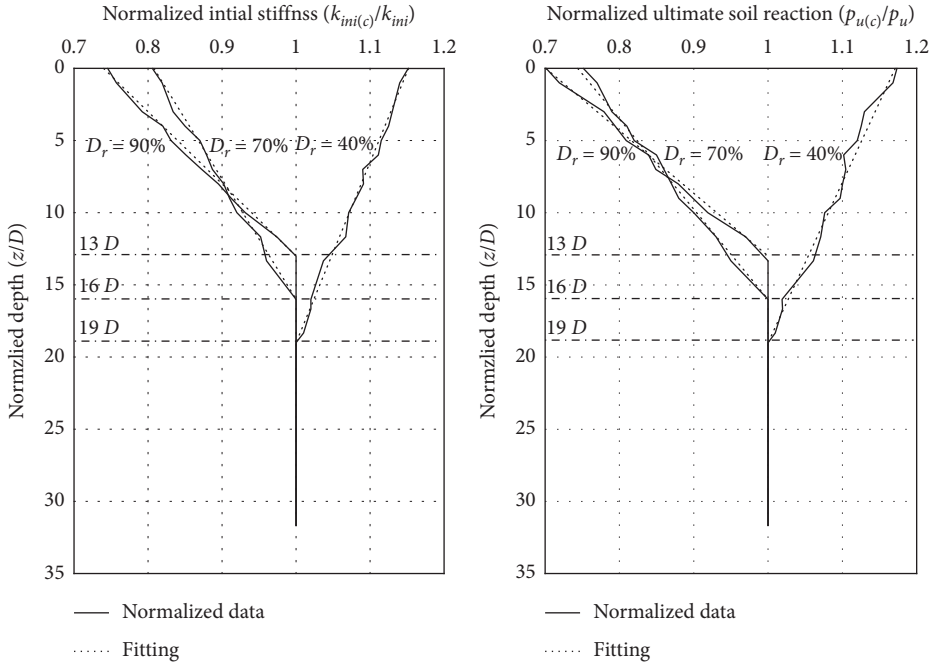

Figure 12: Normalized initial stiffness and normalized ultimate soil reaction versus depth.

stiffness. This is because the larger the cyclic load, the clearer the cyclic loading effect and the greater the impact on the latter part of the p-y curve (i.e., the ultimate soil reaction). The normalized initial stiffness and ultimate soil reaction converge to one. That is, there is no cyclic loading effect below the infinite depth at which lateral displacement did not occur in the model tests (19D, 16D, and 13D for the relative densities of 40%, 70%, and 90%, respectively).

In this study, the normalized initial stiffness and ultimate soil reaction were defined as cyclic loading factors c_i and c_u,

Table 6: Cyclic loading factors for cyclic p-y curves.

Soil conditions	$c_i = k_{ini(c)}/k_{ini}$	$c_u = (p_{u(c)}/p_u)$	Infinite depth
Loose state ($D_r = 40\%$)	$-0.008\ (z/D) + 1.152$	$-0.009\ (z/D) + 1.171$	$19D$
Medium-dense ($D_r = 70\%$)	$0.012\ (z/D) + 0.808$	$0.016\ (z/D) + 0.744$	$16D$
Dense state ($D_r = 90\%$)	$0.020\ (z/D) + 0.740$	$0.023\ (z/D) + 0.701$	$13D$

respectively, and defined as a function of the normalized depth (Table 6). The proposed cyclic loading factors are only effective at depths shallower than the infinite depth and a value of one is applied at depths deeper than the infinite depth.

To summarize the discussion above, the initial stiffness ($k_{ini(c)}$) and ultimate soil reaction ($p_{u(c)}$) of the cyclic p-y curve can be determined by multiplying equations (5) and (6) by the cyclic load factors, respectively. When the calculated $k_{ini(c)}$ and $p_{u(c)}$ are substituted into the hyperbolic equation (4), the cyclic p-y curve can be derived (equation (7)). In this manner, the lateral behaviors (e.g., bearing capacity, displacement, and moment) of a pile installed in saturated silty sand and subjected to cyclic lateral loading can be evaluated.

$$p = \frac{y}{\left(1/k_{ini(c)}\right) + \left(y/p_{u(c)}\right)} = \frac{y}{\left(1/c_i k_{ini(c)}\right) + \left(y/c_u p_u\right)}. \quad (7)$$

6. Comparison to Existing p-y Curves

The p-y curves proposed in this study for SM soil were compared to two existing p-y curves proposed for granular soil. One is the API p-y curve, which is most widely applied in granular soil, and the other is the p-y curve proposed by Baek et al. [5] for Jumunjin silica sand classified as SP using a pile with the same dimensions as those used in this study. Both the p-y curve proposed by O'Neill and Murchinson [1], which is the parent of the API p-y curve and the p-y curve proposed by Baek et al. [5] are silica sand models.

Figures 13(a) and 13(b) present the p-y curves derived by the aforementioned three methods at depths of $2D$ and $4D$ when the model piles used in this study are installed in saturated soils with 40% and 70% relative densities, respectively. The p-y curves proposed in this study and by Baek et al. [5] exhibit two contrasting cyclic loading effects according to the relative density. The stiffness of the p-y curve increases at a relative density of 40%, whereas the stiffness of the p-y curve decreases at a relative density of 70%.

In contrast, when the pile is subjected to cyclic lateral load, the stiffness of the API p-y curve always decreases at a depth of $2D$, but there is no change at a depth of $4D$. This is because the API p-y curve always applies a reduction factor to account for cyclic loading conditions, regardless of the relative density. Furthermore, because the API p-y curve considers the infinite depth at which the effect of the cyclic load is valid as $2.625D$ [34], there is no difference between the static and cyclic p-y curves at a depth of $4D$.

Similar to the aforementioned static loading condition (see Figures 5–7), the API p-y curve under the cyclic loading condition also overestimates the soil reaction under low-load conditions and underestimates the soil reaction under high-load conditions. The magnitudes of the soil reactions of the proposed cyclic p-y curve and API cyclic p-y curve are reversed when loads of 45% ($2D$) and 86% ($4D$) of the static lateral capacity are applied at the relative density of 40% and when loads of 29% ($2D$) and 73% ($4D$) of the static lateral capacity are applied at the relative density of 70%. As mentioned previously, loads much lower than the static lateral capacity (e.g., one-third of the static lateral capacity at a safety factor of 3.0) are considered when an offshore wind power foundation is designed and an even smaller load is applied under actual service loading conditions. In other words, the API p-y curve is considered likely to overestimate the stiffness of the soil springs that are installed in silty sand soil and subjected to cyclic lateral loading.

In a study by Baek et al. [5], which was conducted under the same conditions except for the soil type, the stiffness of the p-y curve increased at a relative density of 40% under cyclic lateral loading, and the stiffness of the p-y curve decreased at a relative density of 70%, representing good agreement with the results of this study. However, the change in the stiffness of the p-y curve under cyclic lateral loading appeared more prominently in the study by Baek et al. [5]. The initial stiffness of the p-y curve increased to 359.2% in soils with a relative density of 40%, whereas it decreased to 77.6% in soils with a relative density of 70%. Particularly when the relative density was 40%, the p-y curve presented by Baek et al. [5] exhibited a significant change in stiffness. It is assumed that the phenomenon of densification of soil around piles was prominent in the silica sand with few fine particles (0% passage through a No. 200 sieve).

Baek et al. [5] also observed stiffness values (initial stiffness and ultimate soil reaction) of both static and cyclic p-y curves greater than those observed in this study. This is because Baek et al. [5] presented a p-y curve for Jumunjin silica sand, which is categorized as SP and has greater shear strength and stiffness than Saemangeum silty sand. The friction angles of Jumunjin silica sands with relative densities of 40% and 70% were 37.3° and 42.0°, respectively [5], which are greater than those of the Saemangeum silty sand (33.9° and 37.5°, respectively) in this study. Furthermore, as shown in Figure 14, as a result of the triaxial compression test conducted at the same restraining pressure of 100 kPa, the initial secant line of the axial strain-deviatoric stress curve was larger in the Jumunjin silica sand. This is because the particle size of the Jumunjin silica sand ($D_{50} = 0.58$ mm) classified as SP is greater than that of the Saemangeum silty sand ($D_{50} = 0.08$ mm) classified as SM. If all other conditions are equal, the soil with a larger particle size has a larger initial interlocking force, and the force per contact is also relatively large [8, 9].

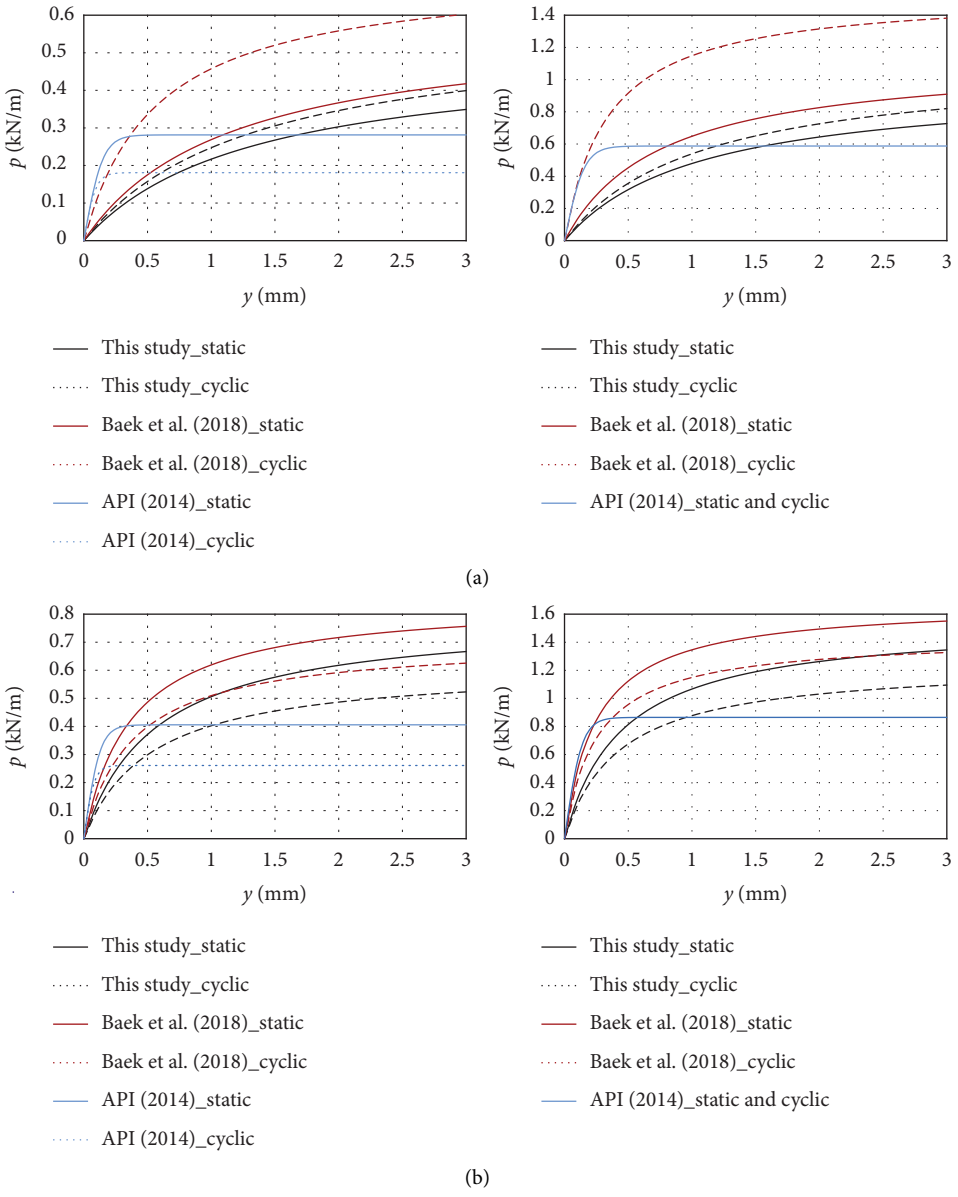

Figure 13: Proposed cyclic p-y curves and existing p-y curves for sandy soils at depths of $2D$ (left) and $4D$ (right). (a) 40%. (b) 70%.

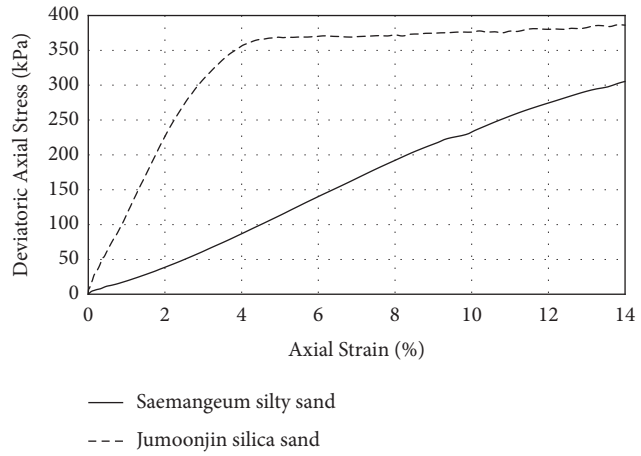

Figure 14: Deviatoric axial stress and axial strain curves of Saemangeum silty sand and Jumunjin silica sand ($D_r = 70\%$).

To summarize the discussion above, when the two existing silica sand models (i.e., API [2] and Baek et al. [5]) were adopted for assessing the pile behavior installed in silty sand, it is highly likely that they would overestimate the static lateral capacity of a pile subjected to cyclic lateral loading. Because the two *p-y* curves (i.e., this study and Baek et al. [5]) proposed under the same conditions except for soil type showed significant differences, the current design method using a representative *p-y* curve, regardless of the type of sandy soil, must be improved. It is expected that the *p-y* curve for silty sand proposed in this study will enable the safe design of offshore foundation structures installed in areas where silty sands are widely distributed, including the target area of the offshore wind farm in the southwestern sea of Korea.

7. Conclusions

This study performed 1g model pile tests to evaluate the *p-y* behavior of pile foundations installed in saturated silty sand and subjected to cyclic lateral loading. Model piles were installed in saturated silty sand with relative densities of 40%, 70, and 90%, and the effects of cyclic lateral loading on the *p-y* behavior of the piles were evaluated by repeatedly applying lateral loads of three magnitudes ($0.3H_{us}$, $0.6H_{us}$, and $0.9H_{us}$) 20 times. The following conclusions can be drawn from this study.

(1) Cyclic lateral loading on piles in loose soil (relative density of 40%) increases the stiffness of the *p-y* curve and decreases the stiffness of the *p-y* curve in dense soils (relative densities of 70% and 90%). This is because in the loose soil (relative density of 40%), repeated lateral loading densifies the soil around piles and improves soil-pile interaction behavior, whereas in the dense soil (relative densities of 70% and 90%), the soil around piles is disturbed (a phenomenon in which the soil in the loading direction is bulged and the soil in the opposite direction to the loading becomes active is repeated), which deteriorate soil-pile interaction behavior.

(2) Static *p-y* curves and cyclic *p-y* curves for silty sand were proposed based on the model test results. The lateral behaviors (e.g., static lateral capacity, displacement, moment) of piles installed in saturated silty sand and dominated by lateral loads can be analyzed using the proposed cyclic *p-y* curves for the pseudostatic analysis of piles.

(3) It was confirmed that the API *p-y* curve and the *p-y* curve proposed by Baek et al. [5] for SP soil are likely to overestimate the lateral support behavior of piles installed in silty sand. This is because these two *p-y* curves were proposed for silica sand that exhibits different behavior compared to the silty sand considered in this study. In silty sand, the increased proportion of fine particles results in a different stress-strain relationship, which results in a smaller stiffness change along the *p-y* curve. Thus, the current design method, which uses the representative *p-y* curve regardless of the type of sandy soil, is not appropriate for evaluating the lateral behavior of piles installed in saturated silty sand.

The findings of this study are expected to be applicable to the evaluation of the behavior of pile foundations subjected to lateral loading in saturated silty sand. In particular, the results of this study were obtained by simulating the soil in the target area of the Southwest Jeollabuk-do Offshore Wind Power Project that is being promoted in South Korea. Therefore, the proposed *p-y* curves can be used as basic data for evaluating the lateral behavior of piles during the construction of offshore wind farms in the future. However, the results of this study were derived using a downscale model experiment under 1g conditions, and the installation methods (e.g., driving or jacking) for piles applied in the field were not considered. The stiffness of the *p-y* curve of driven piles and jacked piles is greater than that of preinstalled piles [3], and the results of preinstalled piles allow for a conservative design; however, the applicability of these research results can be further strengthened if these limitations are overcome through additional model pile tests simulating actual pile installation methods or through a series of field tests.

Data Availability

All data are available from the corresponding author (jykim91@hnu.kr) upon request.

Conflicts of Interest

The authors declare that there are no conflicts of interest regarding the publication of this article.

Acknowledgments

This research was conducted with the support of the "National R&D Project for Smart Construction Technology (No. 22SMIP-A158708-03)" funded by the Korea Agency for Infrastructure Technology Advancement under the Ministry of Land, Infrastructure and Transport, and managed by the Korea Expressway Corporation.

References

[1] M. W. O'Neill and J. M. Murchison, "An evaluation of *p-y* relationships in sands," Research Report No. GT-DF02-83, University of Houston, Houston, Texas, 1983.

[2] L. Marshall, *Geotechnical and Foundation Design Considerations*, American Petroleum Institute, Washington, DC, USA, 2011.

[3] B. Tak Kim, N. K. Kim, W. Jin Lee, and Y. Su Kim, "Experimental load–transfer curves of laterally loaded piles in nak-dong river sand," *Journal of Geotechnical and Geoenvironmental Engineering*, vol. 130, no. 4, pp. 416–425, 2004.

[4] Y. W. Choo and D. Kim, "Experimental development of the *p-y* relationship for large-diameter offshore monopiles in sands: centrifuge tests," *Journal of Geotechnical and Geoenvironmental Engineering*, vol. 142, no. 1, pp. 1–12, 2016.

[5] S. H. Baek, J. Kim, S. H. Lee, and C. K. Chung, "Development of the cyclic *p-y* curve for a single pile in sandy soil," *Marine*

Georesources & Geotechnology, vol. 36, no. 3, pp. 351–359, 2018.

[6] M. Lee, K. Bae, I. Lee, and M. Yoo, "Cyclic *p-y* curves of monopiles in dense dry sand using centrifuge model tests," *Applied Sciences*, vol. 9, no. 8, pp. 1–17, 2019.

[7] M. Y. Fattah, N. M. Salim, and A. M. B. Al-Gharrawi, "Incremental filling ratio of pipe pile groups in sandy soil," *Geomechanics and Engineering*, vol. 15, no. 1, pp. 695–710, 2018.

[8] T. W. Lambe and R. V. Whitman, *Soil Mechanics*, John Wiley & Sons, New York, NY, USA, 1979.

[9] J. T. Han, M. T. Yoo, E. K. Yang, and M. M. Kim, "Evaluation of particle size effect on dynamic behavior of soil-pile system," *Journal of Korean Geotechnical Society*, vol. 26, no. 7, pp. 49–58, 2010.

[10] C. Leblanc, G. T. Houlsby, and B. W. Byrne, "Response of stiff piles in sand to long-term cyclic lateral loading," *Géotechnique*, vol. 60, no. 2, pp. 79–90, 2010.

[11] G. Nicolai and L. B. Ibsen, "Small-scale testing of cyclic laterally loaded monopiles in dense saturated sand," *Ocean and Polar Engineering Conference*, pp. 731–736, 2014.

[12] B. Zhu, B. W. Byrne, and G. T. Houlsby, "Long-term lateral cyclic response of suction caisson foundations in sand," *Journal of Geotechnical and Geoenvironmental Engineering*, vol. 139, no. 1, pp. 73–83, 2013.

[13] J. H. Long and G. Vanneste, "Effects of cyclic lateral loads on piles in sand," *Journal of Geotechnical Engineering*, vol. 120, no. 1, pp. 225–244, 1994.

[14] L. C. Reese and W. F. Van Impe, *Single Piles and Pile Groups under Lateral Loading*, Balkema, Rotterdam, Netherlands, 2001.

[15] S. Iai, "Similitude for shaking table tests on soil-structure-fluid model in 1g gravitational field," *Soils and Foundations*, vol. 29, no. 1, pp. 105–118, 1989.

[16] S. N. Rao, V. G. S. T. Ramakrishna, and M. B. Rao, "Influence of rigidity on laterally loaded pile groups in marine clay," *Journal of Geotechnical and Geoenvironmental Engineering*, vol. 124, no. 6, pp. 542–549, 1998.

[17] K. Jeongsoo, J. Youn-Ju, P. Min-Su, and S. Sunghoon, "Test Bed for 2.5GW Off-Shore Wind Farms at Yellow Sea," Report No. TR.70B9.P2016.0299, KEPRI (Korea Electric Power Cooperation Research Institute), Daejeon, Korea, 2016.

[18] G. G. Meyerhof, "Penetration tests and bearing capacity of cohesionless soil," *Journal of the Soil Mechanics and Foundations Division*, vol. 82, no. 1, pp. 1–19, 1956.

[19] E. K. Yang, *Evaluation of Dynamic P-Y Curves for a Pile in Sand from 1g Shaking Table Tests*, PhD Dissertation, Department of Civil and Environment Engineering, Seoul National University, Seoul, Korea, 2009.

[20] G. G. Meyerhof, S. K. Mathur, and A. J. Valsangkar, "Lateral resistance and deflection of rigid walls and piles in layered soils," *Canadian Geotechnical Journal*, vol. 18, no. 2, pp. 159–170, 1981.

[21] H. L. Davidson, P. G. Cass, K. H. Khilji, and P. V. McQuade, "Laterally loaded drilled pier research," Report No. EPRI-EL-2197-Vol.1, GAI Consultants, Inc, Monroeville, PA, 1982.

[22] W. G. Fleming, A. J. Weltman, M. F. Randolph, and W. K. Elson, *Piling Engineering*, John Wiley & Sons, New York, NY, USA, 2nd edition, 1992.

[23] Y. O. Barton, "Lateral Loading of Model Piles in the Centrifuge," Master Thesis, University of Cambridge, Cambridge, UK, 1979.

[24] M. Heyenyi, *Beams on Elastic Foundation*, University of Michigan Press, Ann Arbor, MI, 1946.

[25] R. F. Scott, *Analysis of Centrifuge Pile Tests; Simulation of Pile-Driving*, California Institute of Technology, Pasadena, CA, USA, 1980.

[26] H. Dou and P. M. Byrne, "Dynamic response of single piles and soil–pile interaction," *Canadian Geotechnical Journal*, vol. 33, no. 1, pp. 80–96, 1996.

[27] K. Abdel-Rahman and M. Achmus, "Finite element modelling of horizontally loaded monopile foundations for offshore wind energy converters in Germany," in *Proceedings of the International Symposium on Frontiers in Offshore Geotechnics*, pp. 391–396, Austin, Texas, 2005.

[28] K. Lesny and J. Wiemann, "Finite Element Modelling of Large Diameter Monopiles for Offshore Wind Energy Converters," in *Proceedings of the GeoCongress*, pp. 1–6, Atlanta, Georgia, April 2006.

[29] G. L. Yoon, S. B. Kim, O. S. Kwon, and M. S. Yoo, "Partial safety factor of offshore wind turbine pile foundation in west-south mainland sea," *Journal of The Korean Society of Civil Engineers*, vol. 34, no. 5, pp. 1489–1504, 2014.

[30] IEC 61400-3, "Wind Turbines – Part 3: Design Requirements for Offshore Wind Turbines," International Standard, DZ, Algeria, IEC 61400-3, 2009.

[31] DNV, "Design of Offshore Wind Turbine Structures," DNV (Det Norske Veritas), Høvik, Norway, DNVOS-J101, 2011.

[32] European Committee for Standardization, "Eurocode 7: Geotechnical Design - Part 1: General Rules," Central Secretariat, Brussels, Belgium, EN 1997-1:2004, 1997.

[33] MOLIT, *Design Standard for the foundation structure of Korea*, MOLIT (Ministry of Land, Infrastructure and Transport), Sejong, Korea, 2016.

[34] S. H. Baek, J. Y. Kim, S. H. Lee, and C. K. Chung, *Effect of Cyclic Lateral Loads on P–Y Curve for Pile Foundations in Saturated Sand*, in *Proceedings of the 25th International Ocean and Polar Engineering Conference*, pp. 983–988, Kona, HI, USA, June 2015.

[35] R. L. Kondner, "Hyperbolic stress–strain response: cohesive soils," *Journal of the Soil Mechanics and Foundations Division*, vol. 87, pp. 115–144, 1963.

[36] L. A. Palmer and J. B. Thomson, "The Earth Pressure and Deflection along the Embedded Lengths of Piles Subjected to Lateral Thrust," in *Proceedings of the 2nd International Conference on Soil Mechanics and Foundation Engineering*, pp. 156–161, Haarlem, Netherlands, June 1948.

[37] J. M. Ting, "Full-scale cyclic dynamic lateral pile responses," *Journal of Geotechnical Engineering*, vol. 113, no. 1, pp. 30–45, 1987.